International Conference on Renewable Energies and Power Quality (ICREPQ'17)
Malaga (Spain), 4th to 6th April, 2017
Renewable Energy and Power Quality Journal (RE&PQJ)
ISSN 2172-038 X, No.15 April 2017

Time-to-Frequency Domain SMPS Model for Harmonic Estimation: Methodology

G. Malagon-Carvajal[1], J. Bello-Pena[2], G. Ordonez-Plata[3], C. Duarte[4]
Department of Electric, Electronic and Telecommunications Engineering
Universidad Industrial de Santander (UIS)
Bucaramanga, (Colombia)
e-mail: {[1]gabriel.malagon, [2]jeisson.bello}@correo.uis.edu.co, {[3]gaby, [4]cedagua}@uis.edu.co

Abstract.— The amount of home appliances based on Switch Mode Power Supply ($SMPS$) systems has increased over the last years. Thus, the harmonic analysis of these loads is useful for the assessment of current distortion in low voltage distribution systems. However, an assessment considering the diversity and attenuation effects represents a challenge on harmonic modeling. This paper proposes a method (T_2FDM) to transform $SMPS$ Time Domain Models (TDM) into Frequency Domain Models (FDM) in order to estimate the input current waveforms when the amplitude, phase angle and distortion of the supply voltage varies (e.g., voltage regulation) around some operating point. The T_2FDM provides the Admittance matrix, which is suitable to assess the impact of household loads with lower computational cost. The method is based on the use of Polar-plots Fingerprints computed from TDMs and not from a large set of measurements. The results from T_2FDM, FDM and TDM are compared against laboratory measurements via the computation of error performance metrics. The study shows that the methodology is appropriate to compute accurate and efficient $FDMs$ from a TDM and a small set of measurements.

Key words

Time Domain Models, Frequency Domain Models, Harmonic Attenuation-Diversity, Admittance Matrix, SMPS.

1. Introduction

Nowadays, electric loads based on power electronics and specifically based on Switch Mode Power Supply ($SMPS$) are widely adopted in residential sector. Many users using different home appliances connected in low voltage grid can inject a significant amount of harmonic currents into the distribution system, especially when these operate under non-sinusoidal grid voltage condition [1], [2]. In this way, the problem of characterizing and modeling residential loads is an important research topic [3]. The references [4]–[6] use sinusoidal, flat-top and pointed-top distorted waveforms voltage supply in order to characterize load input current. However, a few test measurements may be insufficient to describe the load harmonic behavior under variations of the supply voltage. For instance, references [7]–[9] use a measured-based approach composed by extensive field measurements. Among the main advantages for this method are: the model derived is based on real loads measurements and an actual range of voltage supply conditions. Nevertheless, it is possible to obtain inaccurate results for specific loads types in different supply voltage distortions. Moreover, a frequency sweep process based in polar fingerprints is describe in [10]–[15]. In [12] is presented a research about the small photovoltaic inverters characterization and [10] focuses on the interactions between these inverters and the electric vehicles battery chargers ($EVBC$). The test in these works is focused on low order harmonics with four different configuration of voltage supply distortions: single harmonics; combinations of 3rd, 5th and 7th; the fundamental supply fixed and others harmonics orders superimposed; and finally, a random combination of single harmonics. Nevertheless, a comprehensive input current characterization requires to know the load behavior under more voltage operating conditions including regulation voltage and distortion variations . Next, in [13], the experiment is extended up to 19th harmonic order and more of 3000 testing states for the $EVBC$ characterization and in [14], the 11th harmonic order and 144 testing states for frequency domain modeling of household loads. However, the extensive measurements without a automatic control systems for the experiment, it can take a long time. Thus, it would be convenient if a time domain model and a few measurements allow a complete input harmonic current response characterization for loads based on $SMPSs$ in low voltage distribution systems. This paper proposes a method to compute $FDMs$ from TDMs taking into account different operating points for the fundamental voltage amplitude (voltage regulation variation), multiple voltage supply distortions (Until 15th harmonic order) and a few measurements for model testing. The analysis is performed through simulation tools such as MATLAB® script and Simulink® platform. The paper is organized as follows: Section 2 describes the blocks and parameters involved in the TDM. In Section 3 the FDM parameters are explained in detail. Next, in Section 4, the Simulation-Experiment Framework, the Fingerprints polar-plots, the Rectangular $|I|$-$|V|$ Curves and the Admittance Matrix for the proposed method are addressed. In the Results (Section 5) a frequency sweep method is performed. Finally, in Section 6, the conclusions from this research are presented.

2. The SMPS Time Domain Model

The $SMPS$ Time Domain Model (TDM) is presented in Fig. 1. This model is defined by: a rectifier bridge, an input resistance R, an input filter inductance L, a dc link capacitance C_{dc}, and an equivalent resistance R_{eq} [16].

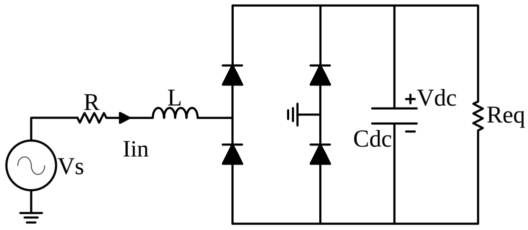

Fig. 1. The SMPS Circuit-Based Model (CBM)

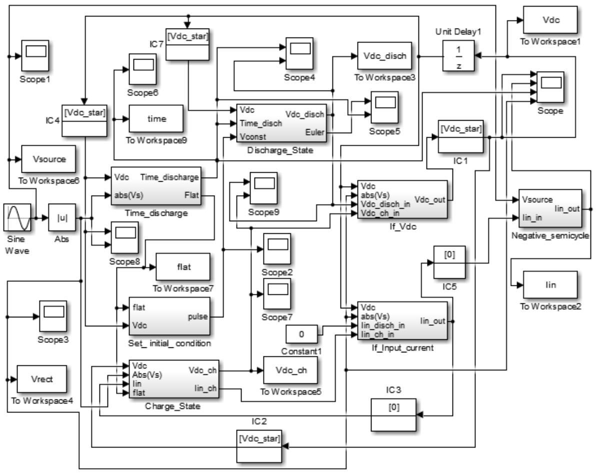

Fig. 2. The SMPS Time Domain Model in Matlab Simulink® Platform

The TDM in Matlab-Simulink® Platform is available in: https://www.mathworks.com/matlabcentral/fileexchange/61601-time-domain-model-for-a-smps–cfl-.

In [16], [17], the state space model and its mathematical disaggregation are analyzed under non-sinusoidal conditions. Summarizing, this model can be stated as:

$$\begin{bmatrix} \frac{\partial i_{in}}{\partial t} \\ \frac{\partial V_{dc}}{\partial t} \end{bmatrix} = \begin{bmatrix} -\frac{R}{L} & -\frac{1}{L} \\ \frac{1}{C_{dc}} & -\frac{1}{R_{eq}C_{dc}} \end{bmatrix} \begin{bmatrix} i_{in} \\ V_{dc} \end{bmatrix} + \begin{bmatrix} \frac{1}{L} \\ 0 \end{bmatrix} V_s \quad (1)$$

This State Space model is implemented in Matlab Simulink® platform for this work (See Fig. 2).

A. SMPS Simulink® Model: Charge_Stage Block

The Charge_State Block is formed by the Subsystem Blocks: Req_ch and Set_initial_condition. The first block models the Discharge Stage resistance ($R_{eq,Charging}$) and the second define the initial conditions of the instantaneous dc link voltage (V_{dc}) in the dc link capacitance (C_{dc}).

B. SMPS Simulink® Model: Discharge_Stage Block

This block models the Discharge Stage resistance, ($R_{eq,Discharging}$) which is defined as a function of the instantaneous dc link voltage (V_{dc}).

C. SMPS Simulink® Model: Time_discharge Block

This block is an arrangement for the transition between charging and discharging states: this block allows comparing the instantaneous dc link voltage (V_{dc}) signal and the rectified supply voltage signal ($Abs(V_s)$) to calculate and reset the time on each state.

D. SMPS Simulink® Model: If_Input_Current Block

If_Input_Current Block is a arrangement that in the same way that the previous block identifies the transition between charging and discharging states by comparing V_{dc} and $Abs(V_s)$. Also, this block compares the discharge state input current (Iin_disch_in) and the charge state input current (Iin_disch_in). It also turns the outputs into action signals in the model process.

E. SMPS Simulink® Model: If_Vdc Block

This block has the same function that the previous one. However, this block also compares the dc link voltage of the discharge state (Vdc_disch_in) and the dc link voltage of charge state (Vdc_ch_in). Additionally, It turns the outputs into action signals in the model process.

F. SMPS Simulink® Model: Negative_semicycle Block

Negative_semicycle block makes the negative semicycle of Out Input current (Iin_out).

3. The SMPS Frequency Domain Model

The Frequency Domain Model (FDM) proposed in this paper is a linear model composed by an input current vector ($\underline{I}_{in(n)}$), an Admittance Matrix ($\underline{Y}^{(\mu,\nu)}_{(n\times n)}$) that describes the behavior of the load, and a vector that defines the supply voltage operation point ($\underline{V}_{s(n)}$) for different harmonics orders (n). The advantage of this model is that it takes into account the variation in the regulation voltage and simplifies its use by the existing methods to solve the harmonic power flow. This model can be defined by the next expression:

$$\begin{bmatrix} I_{in(1)} \\ I_{in(3)} \\ I_{in(5)} \\ \vdots \\ I_{in(n)} \end{bmatrix} = \left[\begin{bmatrix} Y_{1,1} \\ Y_{3,1} \\ Y_{5,1} \\ \vdots \\ Y_{n,1} \end{bmatrix} \begin{bmatrix} Y_{1,3} & Y_{1,5} & \dots & Y_{1,n} \\ Y_{3,3} & Y_{3,5} & \dots & Y_{3,n} \\ Y_{5,3} & Y_{5,5} & \dots & Y_{5,n} \\ & \vdots & & \\ Y_{n,3} & Y_{n,5} & ... & Y_{n,n} \end{bmatrix} \right] \begin{bmatrix} V_{s(1)} \\ V_{s(3)} \\ V_{s(5)} \\ \vdots \\ V_{s(n)} \end{bmatrix}$$
(2)

Where: $[Y_{1,1}\ Y_{3,1}\ Y_{5,1}\ \dots\ Y_{n,1}]' = \underline{Y}^{(\mu,1)}_{(n\times 1)} = \frac{I_{r(n)}}{V_{f(1)}}$

4. The SMPS Time Domain to Frequency Domain Model

A. Simulation-Experiment Framework

The simulation-Experiment Framework is composed by a Programmable AC Voltage Source which allows variations of supply voltage distortion, a $SMPS$ load which corresponds to Equipment Under Test (EUT), the line and source impedances (Z_{LINE}), and a measurement equipment recording voltage and current waveforms.

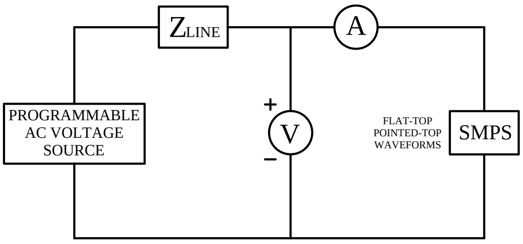

Fig. 3. Simulation-Experiment Framework in order to compute a time-to-frequency domain SMPS model

The $SMPS$ time-domain to frequency-domain modeling, based on simulations and/or measurements, is based on the following procedures:

1) In the first procedure, a nominal fundamental (not distorted) voltage supply is set. Then the voltage regulation and phase angle are gradually varied in a range according to the experiment design (e.g $\pm 8\%$ and/or 0° to 330°).
2) The next procedure fixed the fundamental voltage supply to reference values (nominal amplitude and zero phase). The third harmonic is added to the fundamental voltage (in this work, only odd harmonics are considered) and its magnitude and phase are varied in a range given by the experiment design.
3) The previous procedure is repeated superimposing only one harmonic at a time to the fixed fundamental component. Again, the magnitude and phase angle of the added harmonic are varied in a range following the experiment design.
4) On each procedure the voltage and current response waveforms are recorded.
5) The recorded signals in time domain are transformed to frequency domain in order to compute the voltage and current spectra.
6) Finally, polar and rectangular plots are produced. For each voltage supply set (1^{st}, 1^{st} and 3^{rd}, 1^{st} and 5^{th}, ...) a set of polar-plots or fingerprints indicating magnitude and phase per harmonic current response are drawn (See Section 4-B). The rectangular plots present the $|I|$-$|V|$ relation for a fixed angle of each voltage supply set and a given current order harmonic (See Section 4-C).

B. Fingerprints Indices

The Fingerprint is a polar-plot representation of the harmonic load behavior and the interaction between the voltage supply distortion and the load input current (See Figures 4 and 5). In order to asses the behavior of the harmonic current response, some indices are formulated for Fingerprints currents and voltages in [11]–[15].

The indices are defined to mathematically quantify the total sensitivity of the input current in the fingerprint depending on the variations of the voltage supply distortion, as well as, which elements in the proposed admittance matrix are required to represent the impact of a specific voltage distortion on the harmonic current emission. For the sake of better understanding, in this work, modifications of these indices are proposed.

1) Linearity Index: The Linearity Index [13] is computed as the relation between the distance from the maximum to the minimum currents in a given j-branch of polar fingerprint : $\left|\Delta \underline{I}_{m(j)}^{(\mu,\nu)}\right| = \left|\underline{I}_{j(max)}^{\nu} - \underline{I}_{j(min)}^{\nu}\right|$, and the sum of all distances (d) between successive points of the given j-branch, following the branch from the minimum to the maximum current values: $\sum_{i=1}^{d} \Delta \underline{I}_{i(j)}^{(\mu,\nu)}$. Then, the 25th Percentile is computed over the total number of branches (n) for a specific Fingerprint (μ,ν) (See Equation 3). The closer the index to 1, the stronger the linearity.

$$\underline{L}^{(\mu,\nu)} = P_{25(n)} \left[\frac{\left|\Delta \underline{I}_{m(j)}^{(\mu,\nu)}\right|}{\left|\sum_{i=1}^{d} \Delta \underline{I}_{i(j)}^{(\mu,\nu)}\right|} \right] \tag{3}$$

2) Asymmetry Index: The Fingerprint branches can be asymmetrical [13]. The magnitude asymmetry index $\underline{A}_{\rho}^{(\mu,\nu)}$ computes the ratio of the standard deviation (σ) to the average (μ) of the distance between successive points $\left(\left|\Delta \underline{I}_{i(j)}^{(\mu,\nu)}\right|\right)$ for all the j-branch in the Fingerprint. The phase asymmetry index $\underline{A}_{\phi(j)}^{(\mu,\nu)}$ computes the standard deviation over the average ratio for the angles $\Delta\phi_{m(j)}$ of the lines drawn from the first (minimum current) to the last (maximum current) point in every branch. The 75th Percentile is computed over the total number of branches (n) for a given Fingerprint (μ,ν) (See Equations 4 and 5). The closer the indices to 1, the higher the asymmetry among the branches in the Fingerprint.

$$\underline{A}_{\rho}^{(\mu,\nu)} = P_{75(n)} \left[\frac{\sigma_{\rho(j)}^{(\mu,\nu)}}{\mu_{\rho(j)}^{(\mu,\nu)}} \right] \tag{4}$$

$$\underline{A}_{\phi}^{(\mu,\nu)} = P_{75(n)} \left[\frac{\sigma_{\phi(j)}^{(\mu,\nu)}}{\mu_{\phi(j)}^{(\mu,\nu)}} \right] \tag{5}$$

3) Sensitivity Index: The sensitivity index assess the impact of a distorted voltage on the input current response [13]. If current and voltage harmonic orders are the same, it corresponds to the self-sensitivity index (See Equation 6). On the other hand, the cross-sensitivity index is computed when the harmonic orders are different (See Equation 7). The sensitivity index in milli-Siemens is defined for a given Fingerprint with (n) branches as the ratio of the distance between the first (minimum current) and last (maximum current) j-branch points $\left|\underline{I}_{j(max)}^{\nu} - \underline{I}_{j(min)}^{\nu}\right|$ to the distance between the correspondent voltage supply phasors $\left|\underline{V}_{j(max)}^{\nu} - \underline{V}_{j(min)}^{\nu}\right|$.

$$\underline{S}^{(\nu,\nu)} = \frac{1}{n} \sum_{j=1}^{n} \frac{\left|\underline{I}_{max(j)}^{\nu} - \underline{I}_{min(j)}^{\nu}\right|}{\left|\underline{V}_{max(j)}^{\nu} - \underline{V}_{min(j)}^{\nu}\right|} \times 1000 \tag{6}$$

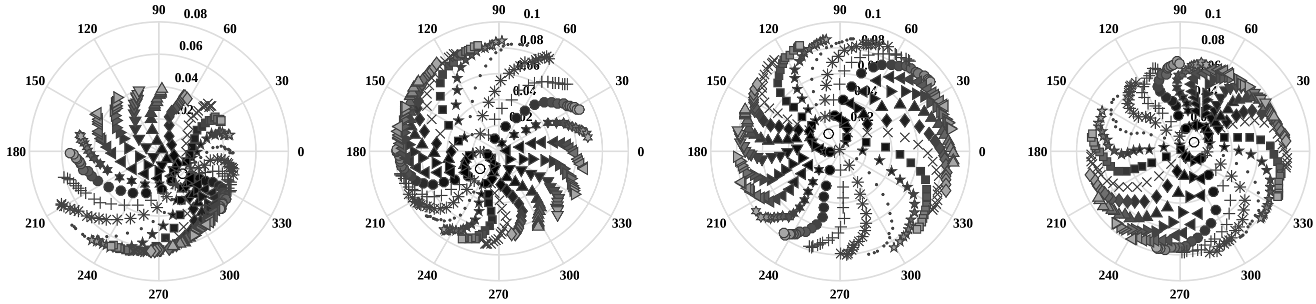

a) Current Response in 9th Harmonic Order b) Current Response in 11th Harmonic Order c) Current Response in 13th Harmonic Order d) Current Response in 15th Harmonic Order

Fig. 4. Polar Fingerprints of harmonic current responses to Fundamental and 13^{th} harmonic Voltage Supply Variation.
Each branch correspond to a fixed angle in the harmonic voltage supply

$$\underline{S}^{(\mu,\nu)} = \frac{1}{n}\sum_{j=1}^{n} \frac{\left|\underline{I}^{\mu}_{max(j)} - \underline{I}^{\mu}_{min(j)}\right|}{\left|\underline{V}^{\nu}_{max(j)} - \underline{V}^{\nu}_{min(j)}\right|} \times 1000 \qquad (7)$$

C. Rectangular $|I|$-$|V|$ curves

The $|I|$-$|V|$ Curves are deployed for each fingerprint branch (j) and represent the behavior of the $SMPS$ input current magnitude when the supply harmonic voltage magnitude varies. For linear loads (e.g. impedances), the $|I|$-$|V|$ curves are expected to be straight lines. For these curves the indices to computed are: the slope or gradient that describe the steepness (m) of the curve $\big(|I|_{\mu} = f(|V|_{\nu})\big)_j$.

D. Admittance Matrix

The admittance matrix proposed in this paper is computed from the analysis of polar-plot fingerprints and rectangular $|I|$-$|V|$ curves. This analysis is based on the Sensitivity index presented in [15] and the Admittance matrix computed from the linearization of each j-branch. Equation (6) resembles the computation of the slope or gradient of the steepness of a straight line, (m). In this way, the $|I|$-$|V|$ curve can be approximated by a straight line with slope (m_Y) $\big((|I|_{\mu} = m_Y|V|_{\nu} + b\big)_j$ using least-squares curve fitting for each j-branch. The slopes (m_Y) for n branches determines the magnitude of an entry in the admittance matrix. On the other hand, the admittance angle is computed from the respective slopes, m_I and m_V, of the fitted lines for each j-branch of the current $((\mu))$ and voltage $((\nu))$ polar fingerprints, respectively. The elements of Admittance Matrix for different harmonics orders are define as:

$$\underline{Y}^{(\mu,\nu)}_{(n\times n)} = \frac{1}{n}\sum_{j=1}^{n} \big[\underline{m}_Y\big]e^{i[\theta Y]}\big]_j \qquad (8)$$

Where:
$\underline{m}_Y$ is calculated from $Fit\big(|I|_{\mu} = m_Y|V|_{\nu} + b\big)_j$,
$\underline{m}_I$ is calculated from $Fit\big(\operatorname{Im}\{I\} = m_I \operatorname{Re}\{I\} + c\big)_j$,
$\underline{m}_V$ is calculated from $Fit\big(\operatorname{Im}\{V\} = m_I \operatorname{Re}\{V\} + d\big)_j$,
$\theta I_{\mu} = tan^{-1}(m_I)$ and
$\theta V_{\nu} = tan^{-1}(m_V)$.

The left column in the admittance matrix must be replaced with $[Y_{1,1}\ Y_{3,1}\ Y_{5,1}\ \dots\ Y_{n,1}]' = \underline{Y}^{(\mu,1)}_{(n\times 1)} = \frac{I_{r(n)}}{V_{f(1)}}$ because the fundamental voltage regulation effect is not considered in [15] (See Section 3).

5. Results

In this section the application of the methodology proposed in Section 4 is illustrated through the computation of the FDM for a 15 W Compact Fluorescent Lamp (CFL). Eight different harmonics are taking into account for the modeling process: 1st, 3rd, 5th, 7th, 9th, 11th, 13th, 15th. Sixteen different, equally separated, voltage magnitude values for each harmonic order are set from 1% to 16% of the fundamental component magnitude. This allows testing up to twice the distortion limits proposed in the IEEE Std 519-2014. Twenty four phase angles, equally separated, are set for fundamental and harmonic components from 15° to 360°. The voltage fundamental component magnitude is set to 16 values, equally separated, from 0% to 8% of the nominal value (230 V for the experiments shown in this paper). In this way, $8 \times 16 \times 24 = 3072$ different voltage operating points are used to simulated the load (CFL). Figures 4 and 5 present the polar-plot fingerprints of the input current response when 3^{rd} and 13^{th} harmonics are superimposed to the fundamental voltage supply, respectively. In these Figures it is possible to observe how the polar-plot fingerprints (a, b, c and d) are highly non-linear. Three models are compared: 1) The $SMPS\ TDM$ fitted and computed from a few measurements [17], 2) the FDM proposed in [15], which is computed from quite a number of measurements, and 3) the time-to-frequency domain model T_2FDM proposed in this article, which computes the FDM from simulations of the TDM for several operating conditions. In order to asses the models performance, the input current of $15W$ CFL is measured under two non-sinusoidal supply voltage waveforms: flat-top (Fig. 6) and pointed-top (Fig. 8) waveforms, which are typical in low voltage distributions systems [4]. The spectra components (See Figures 7 and 9) are computed for the input current and this results are compared with respect to the signal measured using the Error performance metric $(EI_{in(h)})$. This error is defined as the difference between the signal estimated by each model, $(I_{in-sim(h)})$, and the measured one, $(I_{in-meas(h)})$ (See Equation 9 and Table I).

$$EI_{in(h)}[\%] = \left| \frac{I_{in-sim(h)} - I_{in-meas(h)}}{I_{in-meas(h)}} \right| \times 100 \quad (9)$$

From Figures 6 and 8, it is possible to conclude that the models efficiently predict the start and the end of the Charge and Discharge states. The T_2FDM proposed in this paper exhibits the smallest errors when estimating the peak value of the current waveform (0.98% for flat-top and 3.30% for pointed-top) and the fundamental component magnitude (5.50% for flat-top and 5.70% for pointed-top, see Table I). In the flat-top case, the harmonic magnitude estimation error is in the range [3.14-79.82]$\%$ for the TDM, [2.03-68.60]$\%$ for the FDM, and [4.62-41.04]$\%$ for the proposed T_2FDM. Similarly, the angle estimation error is in the range [0.89-229.6]$\%$ for the TDM, [1.24-635.8]$\%$ for the FDM, and [1.83-524.95]$\%$ for the proposed T_2FDM. In the pointed-top case, the harmonic magnitude estimation error is in the range [2.58-111.6]$\%$ for the TDM, [0.02-49.00]$\%$ for the FDM, and [1.12-61.58]$\%$ for the proposed T_2FDM. Similarly, the angle estimation error is in the range [12.15-6063.3]$\%$ for the TDM, [2.77-1744.8]$\%$ for the FDM, and [2.38-1902.2]$\%$ for the proposed T_2FDM.

Table I. - Error of Models in the Harmonic Estimation

Flat-top Voltage Supply						
h	Error in Magnitude [%]			Error in Phase Angle [%]		
o	TDM	FDM	T_2FDM	TDM	FDM	T_2FDM
1	11.86	9.87	**5.50**	**0.89**	1.81	**1.83**
3	9.93	**2.03**	**4.62**	1.42	**1.24**	3.51
5	**3.14**	3.87	10.63	18.80	28.66	22.54
7	48.09	21.55	8.77	21.10	146.69	123.63
9	29.44	6.34	10.26	13.75	16.48	24.02
11	29.96	8.54	24.78	10.62	10.22	14.07
13	5.71	8.70	9.85	17.00	71.64	55.79
15	**79.82**	**68.60**	**41.04**	**229.56**	**635.80**	**524.95**
Pointed-top Voltage Supply [%]						
h	Error in Magnitude [%]			Error in Phase Angle [%]		
o	TDM	FDM	T_2FDM	TDM	FDM	T_2FDM
1	13.02	13.01	**5.70**	**12.15**	3.23	3.33
3	**2.58**	9.80	4.36	12.75	**2.77**	**2.38**
5	28.56	1.17	6.97	70.13	11.63	10.24
7	**111.64**	**49.00**	**61.58**	325.38	110.54	112.04
9	7.97	6.08	5.82	227.89	35.02	32.61
11	19.64	2.37	17.76	82.91	17.85	21.00
13	7.53	2.97	**1.12**	179.22	63.03	60.55
15	29.97	**0.02**	7.33	**6063.3**	**1744.8**	**1902.2**

TDM : [17], FDM: [15], T_2FDM : $Proposed$

6. Conclusion

A Time-to-Frequency Domain Modeling Method is proposed in this paper. The method exploits the advantages of TDMs derived using a small number of measurements in order to estimate the input current when the amplitude (voltage regulation), phase angle and distortion of the voltage supply varies.

The computation of the Admittance Matrix takes into account variations on the fundamental voltage magnitude which is important for assessing the diversity and attenuation-amplification effects with standard harmonic power flow and lower computational cost. The experimental comparison of the proposed method reveals an efficient performance when estimating input current under typical distorted voltage waveforms. However, the estimation of the phase angle for high order harmonics (15^{th}) was not satisfactory for all models, further research about this topic should be performed.

Finally, for future research, a study of Fingerprints related Indices for $SMPS$ can determine which elements in the proposed admittance matrix are required to represent the significant impact of a specific voltage distortion on the harmonic current emission. Likewise, the diversity and attenuation-amplification effects for many loads based on $SMPSs$ should be assessed with the proposed T_2FDM in this paper taking to account the existing methods for harmonic power flow.

Acknowledgment

The authors grateful for the financial support provided by COLCIENCIAS through Convocatoria Nacional No. 567 para estudios de Doctorado en Colombia.

References

[1] P. Ribeiro, J. Leitao, M. Lira, J. Macedo, A. Grandi, A. Testa, R. Langella, J. Cobben, and N. Browne, "Harmonic distortion during the 2010 fifa world cup," in *Power and Energy Society General Meeting, 2011 IEEE*, July 2011, pp. 1–8.

[2] A. M. Blanco, S. Yanchenko, J. Meyer, and P. Schegner, "The impact of supply voltage distortion on the harmonic current emission of non-linear loads," *Dyna*, vol. 82, no. 192, pp. 150–159, 2015.

[3] D. Salles, C. Jiang, W. Xu, W. Freitas, and H. Mazin, "Assessing the Collective Harmonic Impact of Modern Residential Loads;Part I: Methodology," *Power Delivery, IEEE Transactions on*, vol. 27, no. 4, pp. 1937–1946, Oct 2012.

[4] A. Blanco, R. Stiegler, and J. Meyer, "Power quality disturbances caused by modern lighting equipment (cfl and led)," in *PowerTech (POWERTECH), 2013 IEEE Grenoble*, June 2013, pp. 1–6.

[5] A. B. Nassif and J. Acharya, "An investigation on the harmonic attenuation effect of modern compact fluorescent lamps," in *2008 13th International Conference on Harmonics and Quality of Power*, Sept 2008, pp. 1–6.

[6] J. Yong, A. B. Nassif, and W. Xu, "Effect of voltage crest shape on the harmonic amplification and attenuation of diode-bridge converter-based loads," *IET Generation, Transmission Distribution*, vol. 5, no. 10, pp. 1033–1041, October 2011.

[7] V. Cuk, J. F. G. Cobben, W. L. Kling, and P. F. Ribeiro, "Analysis of harmonic current summation based on field measurements," *IET Generation, Transmission Distribution*, vol. 7, no. 12, pp. 1391–1400, December 2013.

[8] M. T. Au and J. V. Milanovic, "Development of stochastic aggregate harmonic load model based on field measurements," *IEEE Transactions on Power Delivery*, vol. 22, no. 1, pp. 323–330, Jan 2007.

[9] A. B. Nassif, J. Yong, and W. Xu, "Measurement-based approach for constructing harmonic models of electronic home appliances," *IET Generation, Transmission Distribution*, vol. 4, no. 3, pp. 363–375, March 2010.

[10] S. Müller, F. Moller, J. Meyer, A. J. Collin, and S. Z. Djokic, "Characterisation of harmonic interactions between electric vehicle battery chargers and pv inverters," in *2014 16th International Conference on Harmonics and Quality of Power (ICHQP)*, May 2014, pp. 645–649.

[11] S. Cobben, W. Kling, and J. Myrzik, "The making and purpose of harmonic fingerprints," in *Proceedings of the 19th International Conference on Electricity Distribution (CIRED)*, 2007, pp. 1–4.

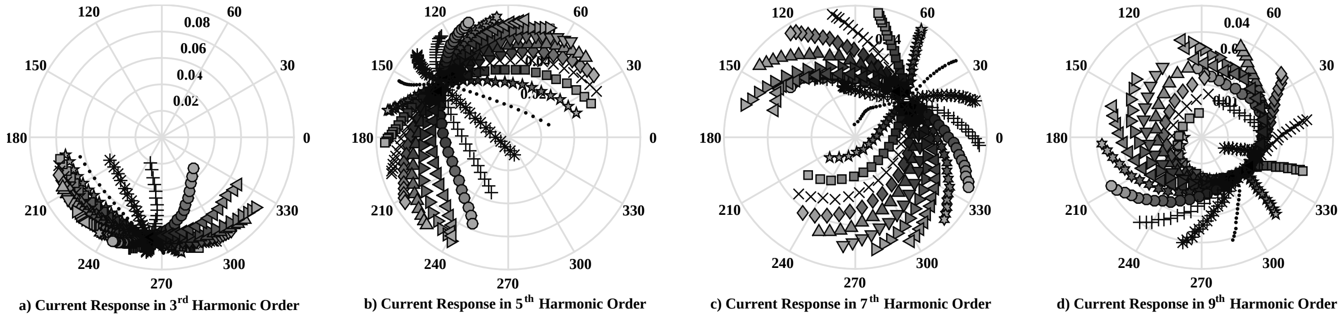

Fig. 5. Polar Fingerprints of harmonic current responses to Fundamental and 3^{rd} harmonic Voltage Supply Variation
Each branch correspond to a fixed angle in the harmonic voltage supply

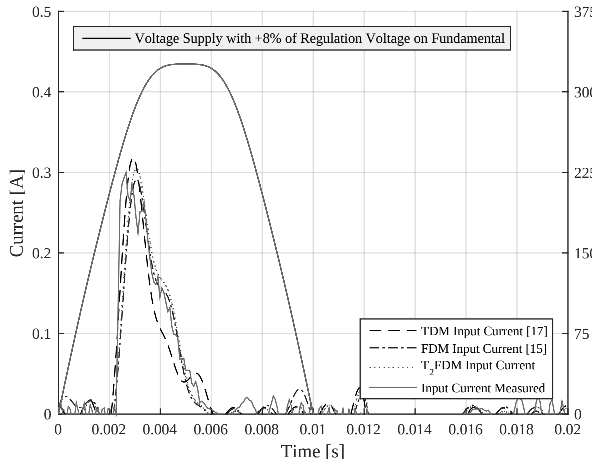

Fig. 6. Input current for $15W$ CFL Flat-top Voltage Supply

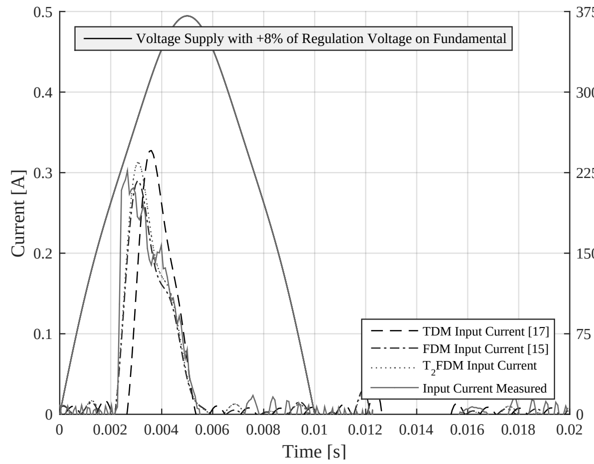

Fig. 8. Input current for $15W$ CFL Pointed-top Voltage Supply

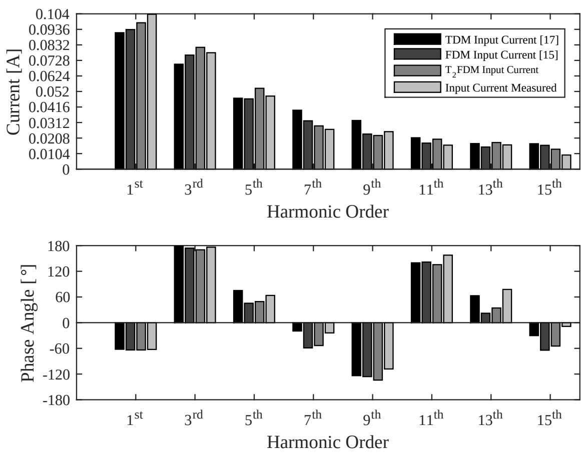

Fig. 7. Input current Spectra for $15W$ Flat-top Voltage Supply

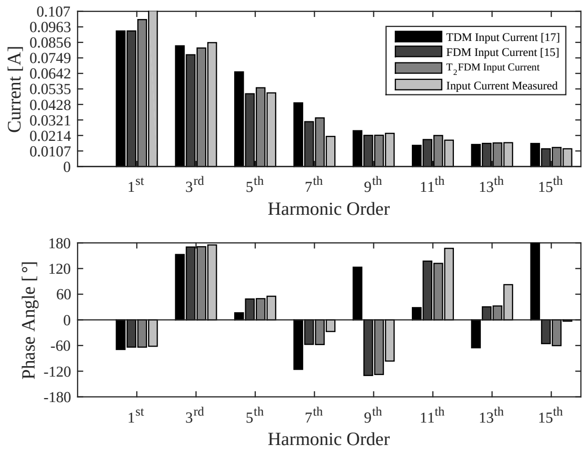

Fig. 9. Input current Spectra for $15W$ Pointed-top Voltage Supply

[12] S. Müller, J. Meyer, and P. Schegner, "Characterization of small photovoltaic inverters for harmonic modeling," in *2014 16th International Conference on Harmonics and Quality of Power (ICHQP)*, May 2014, pp. 659–663.

[13] S. Müller, J. Meyer, P. Schegner, and S. Djokic, "Harmonic modeling of electric vehicle chargers in frequency domain," in *International Conference on Renewable energies and Power Quality (ICREPQ)*, 2015, pp. 1–6.

[14] M. F. Romero, L. Gallego, J. Meyer, and S. Müller, "Characterization of non-linear household loads for frequency domain modeling," *Ingeniería e Investigación*, vol. 35, no. 1Sup, pp. 65–72, 2015.

[15] J. Meyer, S. Müller, P. Schegner, S. Z. Djokic, A. J. Collin, and X. Xu, "Comparison of methods for modelling electric vehicle chargers for harmonic studies," in *2016 Power Systems Computation Conference (PSCC)*, June 2016, pp. 1–7.

[16] G. Malagon-Carvajal, J. Bello-Peña, G. Ordóñez-Plata, and C. Duarte, "Analytical and experimental discussion of a circuit-based model for compact fluorescent lamps in a 60hz power grid," *Ingeniería e Investigación*, vol. 35, no. 1Sup, pp. 89–97, 2015.

[17] G. Malagon-Carvajal, J. Bello-Pena, G. Ordonez-Plata, and C. Duarte, "A comparison between circuit-based and harmonic-current-source models for compact fluorescent lamps," in *17th International Conference on Harmonics and Quality of Power. (ICHQP)*, Oct 2016, pp. 1–7.